

Correlated volumes for extended wave functions on a random-regular graph

Manuel Pino 

Nanotechnology Group, USAL-Nanolab, Universidad de Salamanca, E-37008 Salamanca, Spain;

Institute of Fundamental Physics and Mathematics, E-37008 Salamanca, Spain;

and Institute of Fundamental Physics, CSIC, Calle Serrano 113b, E-28006 Madrid, Spain

Jose E. Roman 

DSIC, Universitat Politècnica de València, Camí de Vera s/n, E-46022 València, Spain



(Received 28 November 2023; accepted 2 April 2024; published 3 May 2024)

We study the metallic phase of the Anderson model in a random-regular graph, specifically the degree of ergodicity of the high-energy wave functions. We use the multifractal formalism to analyze numerical data for unprecedented large system sizes, obtaining a set of correlated volumes N_q which control the finite-size effects of the wave function q moment. Those volumes grow very fast, $\ln[\ln(N_q)] \sim W$, with disorder strength but show no tendency to diverge, at least in an intermediate metallic regime. Close to the Anderson transitions, we characterize the crossover to system sizes much smaller than the first correlated volume. Once this crossover has taken place, we obtain evidence of a scaling in which the derivative of the first fractal dimension behaves critically with an exponent $\nu = 1$.

DOI: [10.1103/PhysRevB.109.184204](https://doi.org/10.1103/PhysRevB.109.184204)

I. INTRODUCTION

Nonergodic and chaotic quantum states exist in some single-particle models with infinite-range connectivity [1–5]. However, its role in realistic many-body systems—those in which interactions have a finite range—has been the subject of intense research in recent years [3,6–10]. To clarify this situation, we can study systems that interpolate between infinite and finite connectivity. That is the case of a particle hopping in a random-regular graph (RRG) in which, although it has finite connectivity, the number of closed loops is small due to the hierarchical structure of the lattice [11,12]. Note that the effect of closed loops is neglected in mean-field theories, the ones that usually explain infinite-dimensional models. Besides its relative simplicity, the hopping process of a particle in a RRG may capture some key ingredients of the effective hopping in the many-body space of interacting Hamiltonians [6,13]. Furthermore, nonergodic and chaotic quantum systems are likely to play an important role in the field of quantum computing [14–19].

The metal-insulator transition in RRGs was recently the subject of deep analysis. The first works on the subject pointed to a nonergodic phase, at least for the metal near the Anderson transition [20–22], which is consistent with its reported slow dynamics [23,24]. However, several other works argued that nonergodicity is a finite-size effect [9,10,23,25–29], which disappear for sizes N larger than a typical volume N_e , referred to as the ergodic volume. Following those references, nonergodicity can still play an important role near the critical disorder W_c as N_e diverges very fast, $\ln(N_e) \sim (W - W_c)^{-1/2}$, upon approaching the Anderson transition [30–32]. Arguments for the ergodicity of the metal are mainly based on the mean-field solutions for the imaginary part of

the local Green's function [9,25,33], which has been obtained with the supersymmetric formalism [34,35] and with population-dynamics-like algorithms [26,28,29,36]. References [26,27,29,32,36] also reported evidence of a divergence in the ergodic volume with exponent $\nu = 1/2$ obtained from exact diagonalization.

Although exact diagonalization has considerably helped us to understand Anderson transitions [37–39], those techniques have not yet given conclusive results regarding the ergodicity of metallic wave functions in RRGs. Indeed, the numerical analysis of those graphs becomes difficult due to large finite-size effects and the need for eigenstate extraction in the middle of the spectrum. Here, we have partially overcome the last limitation using a polynomial filter implemented in the SLEPC libraries [40] to reach much larger sizes than previously obtained, up to $N = 4 \times 10^6$ sites [41]. To deal with the slowness of the finite-size effect, we have developed an accurate procedure to extract the properties of wave functions based on the most general form of the corrections within the multifractal ansatz.

Using the methods described in the previous paragraph, we obtain D_q and their corresponding correlated volumes N_q from the moments of the wave function $I_q = N \langle |\psi_i^{2q}| \rangle$, which are related via $I_q = (N/N_q)^{(1-q)D_q}$. Our results are compatible with an ergodic metal $D_q = 1$ and correlated volumes given by $\ln[\ln(N_q)] \approx W/4 + A_q$ for disorder in the range $5 < W < 15$. The existence of many correlated volumes that are roughly related by $N_q = (N_q)^{c_{qq}}$ implies that there is not a single ergodic volume, but a bunch of correlated volumes N_q that characterize finite-size effects. Alternatively, there is a single graph diameter $\ln(N_q)$ that sets a length scale at which finite-size effects become small. We do not find numerical ev-

idence of diverging correlated volumes for disorders smaller than $W \approx 15$, in contrast to the reported numerical analysis in Refs. [26,28,29,32]. We found that one of the correlated volumes, N_0 , is close to the ergodic volume N_e obtained from Refs. [28,32] but is slightly smaller in the region $W = [13, 15]$. We cannot extract from our fitting procedure any correlated volume closer to the Anderson transition $15.5 < W < W_c \approx 18.1$. This may be due to the correlated volumes becoming much larger than system sizes. But it could also be caused by the existence of a genuine nonergodic metal in this region, as in our procedure we fix ergodicity to produce fits with fewer free parameters. Finally, we find evidence of critical behavior in the first fractal dimension after the crossover $N \ll N_1$ took place, similar to Ref. [42].

II. MODEL AND MULTIFRACTAL ANSATZ

We study the Anderson model [43,44] of a particle hopping between the N nodes of a RRG. That is, we generate a Hamiltonian

$$H = \sum_{i=1}^N \phi_i c_i^\dagger c_i + \sum_{\langle ij \rangle} (c_i^\dagger c_j + c_j^\dagger c_i), \quad (1)$$

where c_i and c_i^\dagger are the destruction and creation operators at site i and ϕ_i are random numbers in $[-\frac{W}{2}, \frac{W}{2}]$, with W being the disorder. The sum on the right-hand side of Eq. (1) runs for all the edges $\langle ij \rangle$ of a graph that is generated following the probability distribution of a RRG with branching number $k = 2$ [45]. Several previous studies agreed that the Anderson transition for this model is at $W_c \approx 18.17$ [10,42,46].

The eigenstates of the Hamiltonian in Eq. (1) are analyzed via the multifractal formalism [47]. We denote the amplitude of eigenstate ψ at site i as ψ_i and assume that the supporting set of sites that scale as $\alpha = -\log_N(|\psi_i|^2)$ is given by $N^{f(\alpha)}$, with $f(\alpha)$ being the multifractal spectrum. The Legendre transforms of f are the multifractal dimensions $D_q = [f(\alpha_q) - \alpha_q q]/(q - 1)$, with $f'(\alpha_q) = q$. An ergodic system implies that $D_q = 1$, while $D_q < 1$ occurs for a nonergodic wave function. We extract D_q averaging the closest to zero wave function moment $I_q = \sum_{i=1}^N |\psi_i|^{2q}$ over Hamiltonian realizations [38,48]. We postulate a scaling form of the effective fractal dimensions $\tilde{D}_q = \log_N I_q / (1 - q)$ given by

$$\tilde{D}_q = \sum_{\substack{j=0, \dots, r \\ k=0, \dots, s}} \frac{a_{jk}^{(q)}}{N^j [\ln(N)]^k}, \quad (2)$$

with r and s being integers. The quantities $a_{jk}^{(q)}$ provide information about the multifractal nature of the wave functions and their finite-size corrections. For instance, fractal dimensions correspond to $D_q = a_{00}^{(q)}$, while we define the q -correlated volume as the exponential of the leading correction $\ln(N_q) = a_{01}^{(q)}$, such that we can express $\tilde{D}_q = D_q [1 - \log_N(N_q)]$ at leading order.

We will fit our numerical data to Eq. (2) with $r = s = 1$ [49] and accept the result if the goodness of the fit is acceptable (see Appendix A for an analysis with $r, s > 1$). The form (2) will also be used for the exponential of the typical value of the wave function $\tilde{\omega}_0 = -(\log_N(|\psi_i|^2))$. Note that this quantity is related to I_q by virtue of $\langle \ln(|\psi_i|^2) \rangle = (I_q/N -$

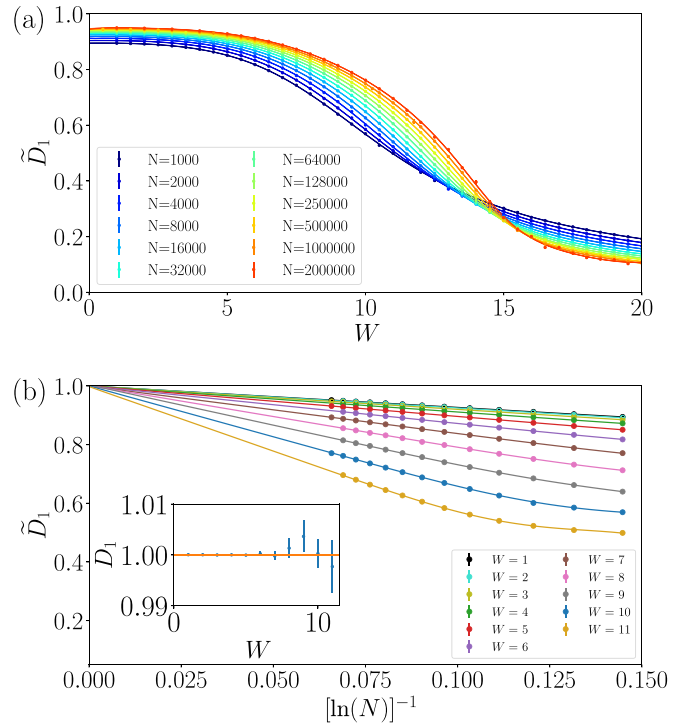


FIG. 1. (a) Effective first fractal dimension $\tilde{D}_1 = S/\ln(N)$, with S being the participation entropy, as a function of disorder strength W for several system sizes N . (b) Effective fractal dimension as a function of system sizes for several values of the disorder between $W = 1$ and $W = 11$. The solid lines fit all data to $\sum_{j=0, k=0}^{r, s} a_{jk}(W)/N^j [\ln(N)]^k$, with $r = s = 1$ for all available sizes at each disorder value $N = 10^3, \dots, 2 \times 10^6$ ($N = 4 \times 10^6$ for $W = 1, 3, 5, 7, 10$). All the fits have p values larger than 0.1, except $W = 2, 6$, which have values that are quite close, $p > 0.07$. The fractal dimension at the thermodynamic limit can be obtained as $D_1 = a_{00}$ (inset).

$1)/q$ in the limit $q \rightarrow 0$. We note that leading finite-size corrections in \tilde{D}_q become negligible when $\ln(N) \gg \ln(N_q)$, so that $\ln(N_q)$ marks the diameter at which \tilde{D}_q is close to its thermodynamics limit value. Those quantities play a role similar to the one attributed to the so-called ergodic volume $N_e = -\ln(\langle \text{Im}G \rangle_{\text{typ}})$ in Refs. [26–28,32] (see Appendix A).

III. FRACTAL DIMENSIONS AND CORRELATED VOLUMES IN THE METAL

We extract D_1 and $\ln(N_1)$ from the data for \tilde{D}_1 . The effective fractal dimension \tilde{D}_1 appears in Fig. 1 as a function of disorder W for sizes $N = 10^3$ to $N = 2 \times 10^6$, together with Padé approximants (solid lines) for each size. The ergodic limit $D_1 = 1$, which, without a doubt, occurs deep enough in the metal, is not reached even for the largest system size at small disorder. However, we can reliably extract fractal dimensions by fitting \tilde{D}_1 for all available sizes via Eq. (2) with $r = s = 1$ [Fig. 1(b)]. The result is compatible with ergodicity $D_1 = 1$ up to the largest disorder computed [inset of Fig. 1(b)]. We note that fitting without the $1/N$ correction produces a very bad quality fit even for small disorders. We have fitted only up to disorder $W = 11$ because the fit for

larger disorder produces too small p values; all p values are reported in Fig. 6 in Appendix B. This implies that larger r and s should be used in order to correctly describe *all* available data sizes for $W \geq 12$.

We focus on the determination of the correlated volumes now. They can be extracted from the effective fractal dimension as the thermodynamic limit of $\ln(\tilde{N}_q) = (D_q - \tilde{D}_q)\ln(N)$. Assuming ergodicity, this formula simplifies to $\ln(\tilde{N}_q) = (1 - \tilde{D}_q)\ln(N)$ for $q > 0$ and to $\ln(\tilde{N}_0) = (-1 + \tilde{\alpha}_0)\ln(N)$ for the logarithm of typical wave functions, which are the quantities shown in Figs. 2(a)–2(c). The solid lines are Padé approximants for each size data set. We repeat the fitting procedure used for D_1 in Fig. 1 for \tilde{D}_2 and $\tilde{\alpha}_0$. In doing so, we obtain extrapolated ergodic values $D_2 = \alpha_0 = 1$ for all the disorders in which corrections in Eq. (2) with $r = s = 1$ produced good quality fits. We also extract $\ln(N_q)$ as the coefficient a_{01} in Eq. (2), which appears in Fig. 2 as stars. We include the ergodic volume N_e (dashed line) extracted from Refs. [32,36] (see Appendix A) and the Gaussian orthonormal ensemble (GOE) value (dot-dashed line).

At small disorder, all the finite-size data in Fig. 2 converge to the corresponding thermodynamic limit extrapolation $\ln(N_q)$ (denoted by stars). The converged values at small disorder fit well with the ones predicted by GOE, while at intermediate values of disorder, $W \approx 10$, they show a behavior given by

$$\ln(N_q) = \exp(A_q + B_q W), \quad (3)$$

with $B_1 \approx 0.235 \pm 0.008$, $B_2 = 0.254 \pm 0.002$, $B_0 = 0.222 \pm 0.005$, $A_1 \approx -1.2$, $A_2 \approx -0.6$, and $A_0 \approx -0.81$. We note that B_q values seem to be close for all the cases considered, but they are not the same. Leaving aside for a moment the small difference in the B_q factors, our results are compatible with a standard critical phenomenon (and also with the supersymmetric formalism [32]) in which the logarithms of all those correlation lengths diverge with an exponent ν . Indeed, all N_q seem to be related by $\ln(N_q) \sim c_{qq'} \ln(N_{q'})$, where the proportionality constant is related to A_q in Eq. (3) as $c_{qq'} = e^{A_q - A_{q'}}$. Returning to the small differences between the B_q factors, these differences imply that the $\ln(N_q)$ factors are not proportional among B_q , which may be because we are not very close to the critical regime.

In this intermediate regime, the slope in double-logarithmic scale of the ergodic volume computed via population dynamics in Ref. [36] (dashed lines in all panels of Fig. 2) is close to $B \approx 0.24$, so $\ln(N_e) \sim \ln(N_q)$ in this regime. Even if we are obtaining results fully compatible with ergodicity $D_q = 1$ for these intermediate disorders, it is not correct to refer to any of the N_q as ergodic volumes, as they set only the system size needed to obtain small leading corrections for the corresponding \tilde{D}_q moment. Indeed, Eq. (3) implies large differences between correlated volumes with different q values.

Note that \tilde{N}_0 in Fig. 2(c) seems to have converged for larger disorders than the ones for which we have reported thermodynamic values. This encourages us to seek alternative fitting procedures to obtain the correlated volume closer to the transition. We tried adding more corrections $r, s > 1$ to Eq. (2), but although we were able to obtain good quality fits by doing so, the addition of more corrections produces nonphysical results

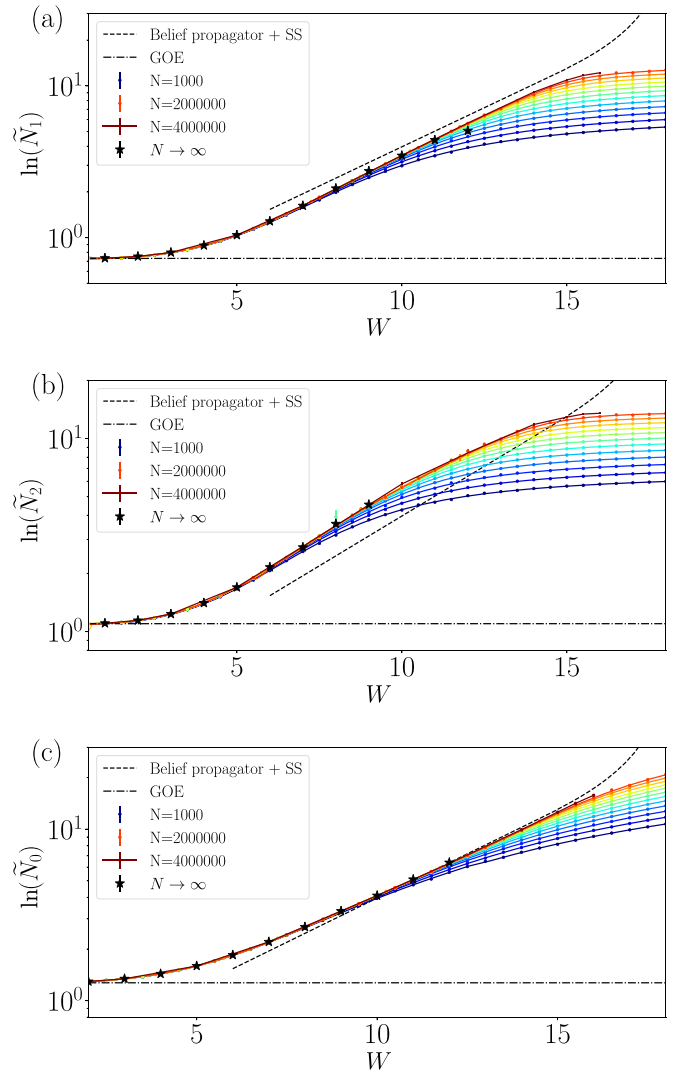


FIG. 2. Finite-size corrections $\ln(\tilde{N}_q)$ assuming ergodicity for (a) $q = 1$, (b) $q = 2$, and (c) $q = M$ as a function of disorder W for several system sizes N . Note the log scale on the y axis. Solid lines are Padé approximants for sizes $N = 10^3, \dots, 2 \times 10^6$, while for $N = 4 \times 10^6$ they are just a guide to the eye. Stars are the value of $\ln(\tilde{N}_q)$ in the thermodynamic limit with the coefficient $\ln(N_q) = a_{01}^{(q)}$ when fitting $\tilde{D}_q = \sum_{j=0, k=0}^1 a_{jk}^{(q)}(W) / \{N^j [\ln(N)]^k\}$ for all the available sizes $N = 10^3, \dots, 4 \times 10^6$ at each disorder value. We do not assume ergodicity for those fits, but we obtain ergodic behavior $D_q = a_{00} = 1$ up to fitting uncertainties. The dashed line is the typical imaginary part of the self-energy obtained via belief propagation and supersymmetric formalism in Refs. [28,32], and the dot-dashed line is the GOE limit.

in the parameter estimation (see Appendix B). Instead, we extract the correlated volume N_0 via a fit of the data without taking into account the smallest sizes while fixing $r = s = 1$ in Eq. (2). The criterion for choosing how many data points are included is based on the minimization of $|1 - \chi_r^2|$. Having a χ_r^2 value close to 1, we are sure that no overfitting occurs. Additionally, we fix the ergodic value $\alpha_0 = 1$ in Eq. (2) to reduce the number of free parameters. See Appendix B for more information on these fits and additional strategies to fit the data.

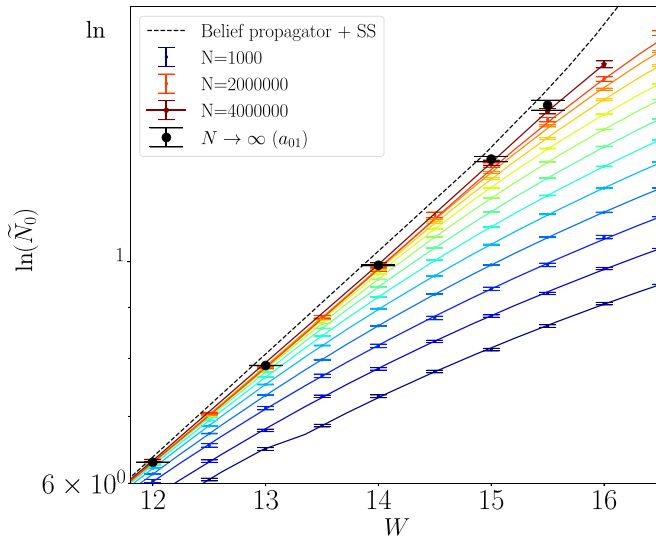


FIG. 3. Finite-size corrections $\ln(\tilde{N}_0)$ assuming ergodicity as a function of disorder for several system sizes from $N = 10^3$ to $N = 4 \times 10^6$. Note the log scale on the y axis. Solid lines are Padé approximants for each size, but the largest one is just a guide to the eye. The circles represent the extrapolated value of $\ln(N_0) = a_{01}^{(0)}$ to the thermodynamic limit via the fit $\tilde{\alpha}_0 = \sum_{j=0, k=0}^1 a_{jk}^{(0)} / \{N^j [\ln(N)]^k\}$, where the ergodic value $a_{00}^{(0)} = \alpha_0 = 1$ is fixed. Several of the smaller sizes were removed for each disorder to obtain good quality fit $p > 1$; for instance, five are used for $W = 15.5, 16$. The dashed line is the typical imaginary part of the self-energy [28,32].

A zoom of $\ln(\tilde{N}_0)$ appears in Fig. 3 for the finite system, together with its extrapolated value $\ln(N_0)$ (black circles) up to disorder $W = 15.5$. Note that the fit for this disorder includes only the four largest sizes (see Fig. 8 in Appendix B), which produces a large error bar for the corresponding extrapolation. The analytical estimation N_e (dashed line) is larger than our infinite-size extrapolated N_0 for $W > 13$. The differences between the two estimations become more pronounced at large disorder $W \approx 15$, the disorder at which the tendency of N_e begins to exhibit a tendency to diverge. We cannot conclude whether the correlated volume $\ln(N_0)$ extracted from our numeric at $W = 15.5$ is still described by Eq. (3) or whether it begins to deviate from that law due to the uncertainty in its extrapolation. In any case, no sign of divergence at criticality can be inferred from our correlated volume. Thus, exact diagonalization results up to $N = 4 \times 10^6$ do not provide evidence of divergence in the correlated volumes, specifically, none with exponent $\nu = 1/2$, in contrast to Refs. [10,28–30,32]. We note that the small differences in the slopes on the log-log plot of correlated volumes versus disorder are evident here. Indeed, the correlated volume N_0 shows a slope on a double-log scale that is definitely different from the analogous ones for the so-called ergodic volume N_e .

IV. FINITE-SIZE EFFECTS NEAR THE ANDERSON TRANSITION

As we have seen, our finite-size numerical results up to $N = 4 \times 10^6$ do not contain indications of divergences in N_q or of a critical exponent $\nu = 1/2$. One of us reported additional

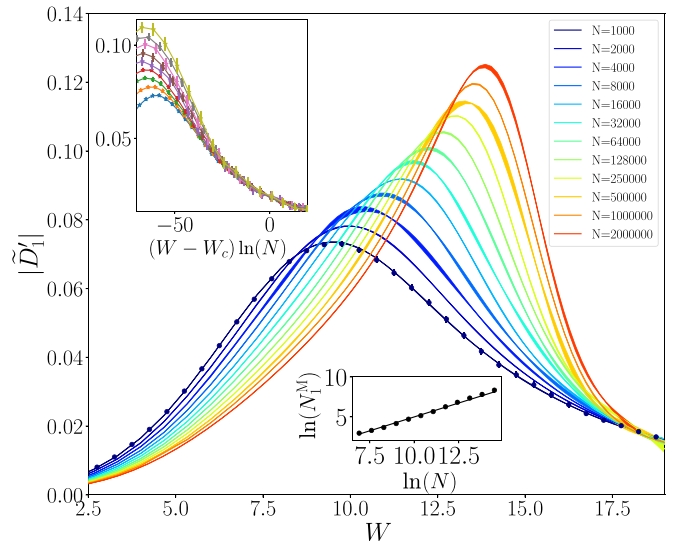


FIG. 4. Absolute value of the derivative $\frac{d\tilde{D}_1}{dW}$ as a function of disorder W . Solid lines are the derivative of the Padé approximant for \tilde{D}_1 . The numerical derivative of \tilde{D}_1 is included for the smallest size to check the consistency with its corresponding Padé derivative. Top inset: numerical derivative of \tilde{D}_1 near the Anderson transition $W_c \approx 18.17$ for sizes up to $N = 128\,000$. Bottom inset: estimation of the logarithm of the first correlated volume $N_1^M = A_1 + BW$, with $A_1 = -1.2$ and $B = 0.24$ [see Eq. (3)] at the disorder where a maximum occurs at \tilde{D}_1 for a given size N (see main panel) as a function of the logarithm of the system size. The solid line fits to $a \ln(N) + b$, yielding $a \approx 0.7$, $b \approx -2$.

evidence of a critical scaling in the derivative of the fractal dimensions, not in the correlated volumes [42]. In that work, the derivative of the first fractal dimension was found to display a crossing point for curves corresponding to different sizes, so that a nonanalyticity with a continuous D_1 and exponent $\nu = 1$ seemed to develop at the Anderson transition. Here, we check that our data up to $N = 250\,000$ are still compatible with such a scaling (error bars are too big for larger system sizes) and that this critical scaling appears only when the crossover to $N \ll N_1$ has taken place.

In Fig. 4 we plot the derivative of the Padé approximants of the first fractal dimension for lengths up to $N = 2 \times 10^6$. Maxima occur for all the sizes at intermediate values of disorder from $W = 10$ to $W = 15$, around the same disorder at which finite-size effects begin to become important in $\ln(\tilde{N}_1)$ in Fig. 2(a). We can extract the correlated volume at each of the maxima $N_1^M(N)$ using Eq. (3) with the disorder $W_M(N)$ at which the maxima occur for a given size N . In doing so, we are able to check that the maxima occur when $\ln(N_1^M) \sim 0.7 \ln(N)$, as shown in the bottom inset of Fig. 4. Taking the number of nodes in the RRG as the size $L \sim \ln(N)$, this implies that the crossover is controlled by the diameter of the graph $L \sim \ln(N)$, not by its volume [50]. Such a crossover occurs for the correlated volumes because they grow very fast [Eq. (2)], even if there is no evidence of a divergence as in a standard second-order phase transition.

Besides the crossover we have already commented on, there is an additional critical behavior in a RRG with exponent $\nu = 1$. This can be seen in the top inset of Fig 4, where all the

curves for the first fractal dimension collapse when plotted as a function of the scaling variable $\ln(N)(W - W_c)^{1/\nu}$, with $\nu = 1$. We have not attempted to fit our data to a scaling form as in Ref. [42] because the data D'_1 for the larger sizes do not contain enough disorder realizations to give accurate results. Note that the region of this critical scaling—the region where the curves for different sizes collapse into a single curve—never occurs for disorder around the maximum. Thus, the additional critical scaling with $\nu = 1$ occurs only once the crossover has taken place.

V. SUMMARY AND CONCLUSIONS

We have analyzed the Anderson problem in a RRG with different quantities, the correlated volumes, taking advantage of polynomial filters implemented in SLEPC. Using them, we obtained results compatible with ergodicity $D_q = 1$ and correlated volumes growing fast, $\ln[\ln(N_q)] \sim W/4$, in an intermediate metallic regime. The zero correlated volume is similar to the ergodic volume N_e found with the typical value of the local density of states in Refs. [28,29,32]. We showed further evidence of critical behavior with $\nu = 1$ in \tilde{D}'_1 once the crossover $\ln(N) \ll \ln(N_1)$ has taken place. As we did not obtain evidence of divergence for correlated volumes, we cannot validate the picture of a critical exponent $\nu = 1/2$ derived from the supersymmetric formalism [30–32]. Taking into account that our system sizes are much larger than the ones used in previous works, previous evidence of such a divergence from exact diagonalization results should be revised.

Several scenarios are compatible with our data. The most standard one is that the self-consistent approximation for the probability distribution of the Green's function holds. Then, a divergence of correlated volumes can occur with $\nu = 1/2$ for larger disorder values than the one for which we can reliably extract correlated volumes, $W \approx 15$. If this is the case, the situation will be fully described by the supersymmetric formalism, and as a result, the full metal may become ergodic [10,30,32,33]. Note that, in this case, the additional critical behavior in D'_1 near the Anderson transition (see Sec. IV) may be a consequence of the Bethe and random-regular graphs' equivalence for sizes much smaller than the first correlated volume, similar to what was discussed in Ref. [25]. Then, we can talk about an ergodic diameter, not an ergodic volume, as $\ln(N_e)$ marks the scale of the graph diameter from which finite-size corrections to the thermodynamic result vanish for all I_q . Even in this scenario, there are still details that we need to understand better, such as the differences between the slopes of correlated volumes in double-logarithmic scale as a function of disorder strength for different q [see Eq. (3) and Figs. 2 and 3]. As a consequence, note the differences between the thermodynamic values of the correlated volume N_0 (circles) and the ergodic volume computed from the self-consistent solution (dashed line) in Fig. 3. Closed loops in the self-consistent equations may help to clarify this [51].

Another scenario compatible with our numerical data is that at disorder $15 < W < W_c$ there is a genuine nonergodic regime in which part of the fractal dimension becomes smaller than its ergodic value $D_q < 1$. Note that none of our results for $\ln(\tilde{N}_0)$ in Fig. 2 show clear convergence with system size for

disorder $W > 15.5$. This may be an indication that $\alpha_0 > 1$ has a nonergodic value in the thermodynamic limit, which implies $\ln(\tilde{N}_0) \sim \ln(N)$. This is an interesting case worth analyzing further. It would imply that the self-consistent approximation that leads to the analytical supersymmetric formula [30,32] does not capture the multifractal character of the wave functions. This situation may be similar to the one that occurred in spin glasses on a RRG 20 years ago [12] (see [22]).

Although we have analyzed large graphs, an effort should be made to go for even larger ones. We are confident that our numerical method will still work for sizes $N = 8 \times 10^6$ or even larger. Besides disordered RRGs, we believe that the numerical methods together with the improved finite-size analysis employed here will be beneficial for a large class of problems involving disordered systems.

ACKNOWLEDGMENTS

We thank A. Rodríguez for useful discussions. M.P. and J.E.R. acknowledge support by the Spanish MCIN/AEI/10.13039/501100011033 through Grants No. PID2020-114830GB-I00 and No. PID2022-139568NB-I00, respectively. M.P. further acknowledges funding from the European Commission FET-Open project AVaQus GA 899561 and from MCIN/AEI/10.13039/501100011033 together with European Union NextGenerationEU/PRTR project Consolidación Investigadora CNS2022-136025. The computational experiments were carried out on the supercomputer Tirant III belonging to Universitat de València and SCAYLE, Supercomputación Castilla y León.

APPENDIX A: CORRELATED VOLUME FROM THE IMAGINARY PART OF THE GREEN'S FUNCTION

We explain how we interpolated previous results obtained by Biroli and Tarzia via population dynamics [28] and the ones by Tikhonov and Mirlin using the supersymmetric formalism [32]. From Eq. (23) in [32], the correlated volume is computed up to second order near the Anderson phase transition $W_c = 18.17$ from the typical value of the imaginary part of the diagonal Green's function:

$$\langle \text{Im}G^- \rangle_{\text{typ}} = e^{-[a_1(W_c - W)^{1/2} + a_2(W_c - W)^{3/2}]^{-1}}, \quad (\text{A1})$$

with $a_1 = 0.0313$ and $a_2 = 0.00369$. The ergodic volume can be extracted as $\ln(N_e) = -\ln(\langle \text{Im}G^- \rangle_{\text{typ}})$, which is related to the typical value of the local density of states $\rho_{E=0}(r)$ in the middle of the spectrum as $\rho_E(r) = \mp \text{Im}G^{(\pm)}(r, r)/\pi$. The same quantity can be obtained via population dynamics algorithms which, roughly speaking, numerically find a distribution probability that solves the self-consistent equations in the Bethe lattice for the Green's function [52]. In doing so, Biroli and Tarzia obtained the diagonal part of G^- and thus its typical value, a few points (red circles) of which are shown in Fig. 5(a). We fit those points to a linear function in double-log coordinates on the x axis. The result is represented as a red solid line. In the same panel, we show the supersymmetric law (A1) [32] as a blue solid line from $W = 12$ to $W = 18$.

The result from Eq. (A1) [dashed blue line in Fig. 5(a)] has a different tendency for disorder around $W \approx 12$ than the

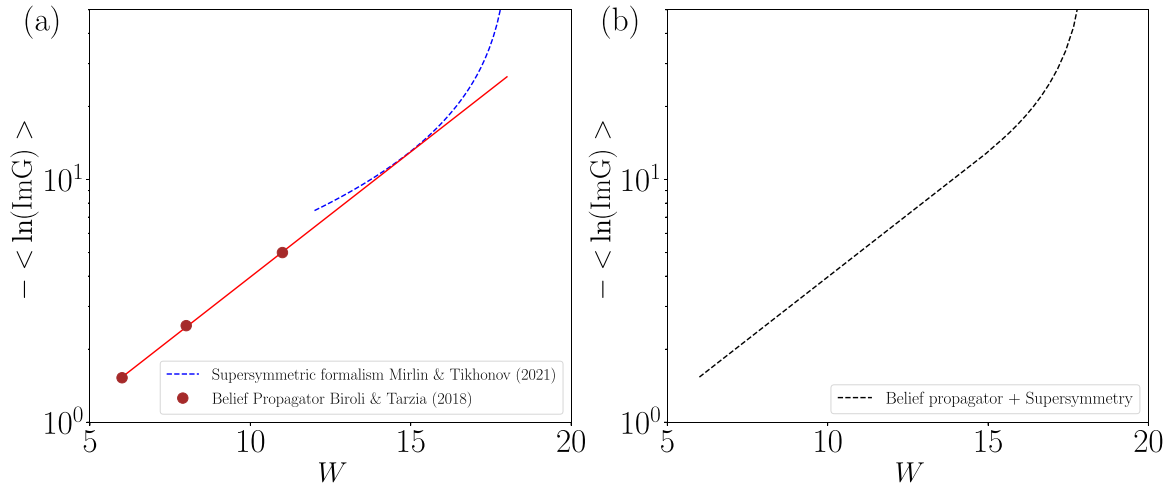


FIG. 5. (a) Mean-field results for minus the logarithm of the typical value for the imaginary part of Green's function in a random-regular graph with branching number $k = 2$. The circles are the results from population dynamics contained in Ref. [28]. The red solid line is an extrapolation of these points to a straight line with a slope of approximately 0.24. The blue solid line is obtained via the supersymmetric formalism (23) of Ref. [32]. (b) Interpolation of the results for the population dynamics of Ref. [28] in the range $W \in [6, 15]$ and the supersymmetric formalism in the range $W \in [15, 18.2]$.

linear tendency of the data from Biroli and Tarzia [solid red line in Fig. 5(a)]. This is not a surprise because the supersymmetric formula is valid only close enough to the transition because it is a second-order expansion in $(W - W_c)^{-1/2}$. Thus, we take as valid the extrapolated line for the belief propagator data from Ref. [28] at small disorder and the supersymmetric formula at larger disorder. We take the point where the solid and dashed lines in Fig. 5(a) coincide as separating the region of validity for each of the laws. We reconstruct the “mean-field” solution as the line in Fig. 5(b), which is the one shown in several of the plots in the main text. We checked that the

results from the population dynamics contained in Ref. [32] are very well described by this reconstruction of the mean-field solution.

APPENDIX B: ANALYSIS OF THE FINITE-SIZE CORRECTIONS TO FRACTAL DIMENSIONS AND THE MULTIFRACTAL SPECTRUM MAXIMUM

We explore different functional forms to fit effective fractal dimensions $\tilde{D}_q = \log_N(I_q)/(q - 1)$ and the exponential of the typical value of the wave function amplitude $\tilde{\alpha}_0 =$

W	D_1	ΔD_1	χ_r^2	p-value
1	1.00004e+00	2e-05	0.8	0.62
2	1.00003e+00	4e-05	1.81	0.07
3	9.9999e-01	2e-05	1.28	0.24
4	1.00001e+00	6e-05	0.93	0.49
5	9.9996e-01	7e-05	1.41	0.18
6	1.0002e+00	2e-04	1.86	0.06
7	9.998e-01	4e-04	0.74	0.67
8	1.0013e+00	9e-04	0.68	0.71
9	1.004e+00	2e-03	1.7	0.09
10	1.000e+00	1e-03	0.78	0.64
11	9.98e-01	3e-03	0.64	0.75
12	9.57e-01	4e-03	6.6	0.0

FIG. 6. Additional information for the fits of the effective first fractal dimension $\tilde{D}_1 = S/\ln(N)$, with S being the participation entropy, to the law $\sum_{j=0, k=0}^{r,s} \frac{a_{jk}(W)}{N^j [\ln(N)]^k}$, with $r = s = 1$ for sizes $N = 10^3, \dots, 4 \times 10^6$ and several values of the disorder W . The first column shows the disorder, the second (third) shows fractal dimensions (errors) extracted from the fitting parameters as $D_1 = a_{00}$. The last two columns show the reduced χ^2 and the p value of each fit.

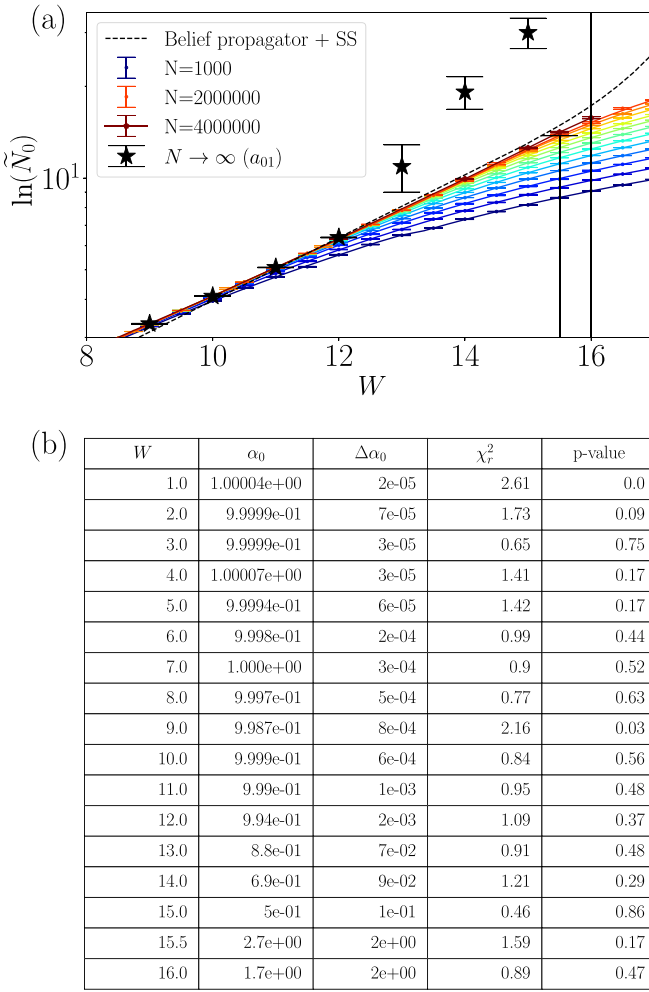


FIG. 7. (a) Logarithm of the effective correlated volume $\ln(\tilde{N}_0)$ as a function of disorder for several system sizes. The dashed line is the typical imaginary part of the self-energy obtained via belief propagation and supersymmetric formalism in Refs. [28,32]. Stars are the values of $\ln(\tilde{N}_q)$ in the thermodynamic limit extracted from the coefficient $\ln(\tilde{N}_0) = a_{01}^{(0)}$ when fitting $\tilde{\alpha}_0 = \sum_{j=0,k=0}^1 a_{jk}^{(0)}(W)/\{N^j[\ln(N)]^k\}$ for all the available sizes $N = 10^6, \dots, 4 \times 10^4$ at each disorder value. r and s are chosen to minimize $|1 - \chi_r^2|$, where χ_r^2 is the reduced chi-square statistic. That is, $r = s = 1$ up to $W = 12$, $r = 1$ and $s = 2$ in the range $12 < W < 15$, and $r = s = 2$ for the largest disorder. (b) Parameters of the fits. The first column shows the disorder, the second and third show the spectrum maximum and its errors, and the last two columns show the reduced χ^2 and the p value of each fit.

$\langle \log_N(|\psi|^2) \rangle$). The N dependence of those two quantities is captured by Eq. (2). However, we can set only a reduced number of terms in those expressions in order to avoid an overfit due to the limited number of data points available. We comment here on how many and which corrections should be included to obtain reliable thermodynamic extrapolations. We also provide additional information about the fits shown in Fig. 1.

We begin with the details of the fit for \tilde{D}_1 in Fig. 1. The data for this quantity were fitted to Eq. (2) with $r = s = 1$. In Fig. 6, we show additional information regarding that fit. As

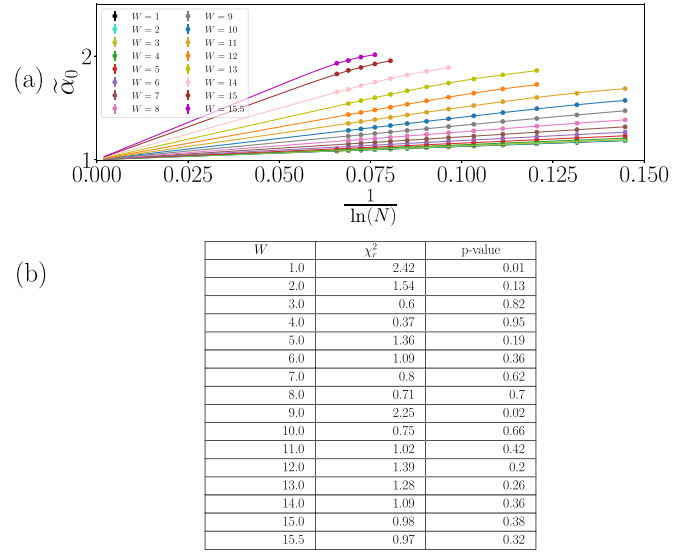


FIG. 8. (a) Logarithm of the effective location of the multifractal spectrum $\tilde{\alpha}_0 = \langle \log_N(|\psi|^2) \rangle$ as a function of $1/\ln(N)$, with N being the system size. Solid lines are a fit of the data to the law in Eq. (2) with the ergodic value fixed at $a_{01} = 1$ and corrections $r = s = 1$. The number of points that are fitted are those which produced the closest to one χ_r^2 . (b) Parameters of the fits. The first column shows the disorder, the second shows the reduced χ^2 , and the third shows the p value of each fit.

explained in the main text, the quality of the fit is good up to $W = 12$, where the smallness of the p value implies that our law does not capture the size dependence of our data. Almost all the extracted fractal dimensions with acceptable goodness of fit (p values larger than 0.1) are consistent with $D_1 = 1$. Thus, the data set for which the goodness of fit is acceptable gives meaningful parameter results, as we expect to have ergodicity $D_1 = 1$ deep enough in the metal. We will see in the next paragraph that this is not the case when fitting with corrections different from $r = s = 1$.

Now we comment on the fits to extract the multifractal spectrum maximum α_0 and its associated correlated volume \tilde{N}_0 . We saw in the main text that $\tilde{\alpha} = \langle \log_N(|\psi|^2) \rangle$ shows small finite-size effects for the largest sizes up to disorder $W = 15$. Nevertheless, we have been able to obtain acceptable fits of $\tilde{\alpha}_0$ to the law in Eq. (2) only up to $W = 12$ in Fig. 2. This is, in part, due to the way we perform the fits with all available sizes and use only a small number of corrections in Eq. (2), indeed, those with $r = s = 1$. It is clear that a larger number of corrections is needed when approaching the Anderson transition. Thus, our first procedure to extract the thermodynamic limit extrapolation is to increase the number of corrections. We do so by using values of r and s that produce the fit with the reduced- χ^2 statistic closest to 1 [53]. Figure 7(a) shows the extrapolated value of the fits for the logarithm of the zero-correlated volume $\ln(\tilde{N}_0)$. It produces values that are not expected at all on physical grounds. Besides a too large correlated volume $\ln(\tilde{N}_0)$, note the log scale on the y axis of Fig. 7(a); it predicts the position of the multifractal spectrum $\alpha_0 < 1$, which is not possible [see Fig. 7(b)]. We remark that no hint of a poor quality fit can be inferred from the p value or the χ_r^2 statistics for the fits that provided nonphysical results

[see Fig. 7(b)]. This is different from results mentioned in the previous paragraph, in which nonphysical results could be mostly pointed out by bad quality fits.

Like in the previous discussion, we obtained good quality fits whose parameters are nonphysical when fitting fractal dimensions D_q with $q = 1, 2$ with $r, s > 1$ in Eq. (2). This behavior should be attributed to the slowness of the corrections given by a power law in $1/\ln(N)$, and it is the reason why we prefer to fit the number of corrections and allow a smaller number of data points. As explained in the main text,

we fitted numerical results for $\tilde{\alpha} = \langle \log_N(|\psi|^2) \rangle$ to Eq. (2) of the main text with fixed $r = s = 1$ but employed only the largest system sizes in order to obtain the χ_r^2 closest to 1. To help the fitting procedure, we also fixed the thermodynamic value $\alpha_0 = 1$ in the fitting law. With this procedure we obtained the correlated volume N_0 displayed in Fig. 3. We provide additional information about those fits in Fig. 8 as the p value or the χ_r^2 statistics. Note that χ_r^2 does not indicate an overfit for any of the disorder values [second column of Fig. 8(b)].

-
- [1] M. Aizenman and S. Warzel, Extended states in a Lifshitz tail regime for random Schrödinger operators on trees, *Phys. Rev. Lett.* **106**, 136804 (2011).
- [2] S. Warzel and M. Aizenman, Resonant delocalization for random Schrödinger operators on tree graphs, *J. Eur. Math. Soc.* **15**, 1167 (2013).
- [3] V. E. Kravtsov, I. M. Khaymovich, E. Cuevas, and M. Amini, A random matrix model with localization and ergodic transitions, *New J. Phys.* **17**, 122002 (2015).
- [4] I. Khaymovich and V. Kravtsov, Dynamical phases in a “multifractal” Rosenzweig–Porter model, *SciPost Phys.* **11**, 045 (2021).
- [5] M. Pino, J. Tabanera, and P. Serna, From ergodic to non-ergodic chaos in Rosenzweig–Porter model, *J. Phys. A* **52**, 475101 (2019).
- [6] B. L. Altshuler, Y. Gefen, A. Kamenev, and L. S. Levitov, Quasiparticle lifetime in a finite system: A nonperturbative approach, *Phys. Rev. Lett.* **78**, 2803 (1997).
- [7] M. Pino, L. B. Ioffe, and B. L. Altshuler, Nonergodic metallic and insulating phases of Josephson junction chains, *Proc. Natl. Acad. Sci. USA* **113**, 536 (2016).
- [8] D. Venturelli, L. F. Cugliandolo, G. Schehr, and M. Tarzia, Replica approach to the generalized Rosenzweig–Porter model, *SciPost Phys.* **14**, 110 (2023).
- [9] K. S. Tikhonov, A. D. Mirlin, and M. A. Skvortsov, Anderson localization on random regular graphs, *Phys. Rev. B* **94**, 220203(R) (2016).
- [10] K. S. Tikhonov and A. D. Mirlin, Critical behavior at the localization transition on random regular graphs, *Phys. Rev. B* **99**, 214202 (2019).
- [11] S. N. Dorogovtsev, A. V. Goltsev, and J. F. F. Mendes, Critical phenomena in complex networks, *Rev. Mod. Phys.* **80**, 1275 (2008).
- [12] M. Mézard and G. Parisi, The Bethe lattice spin glass revisited, *Eur. Phys. J. B* **20**, 217 (2001).
- [13] D. Basko, I. Aleiner, and B. Altshuler, Metal-insulator transition in a weakly interacting many-electron system with localized single-particle states, *Ann. Phys. (NY)* **321**, 1126 (2006).
- [14] B. Altshuler, H. Krovi, and J. Roland, Anderson localization makes adiabatic quantum optimization fail, *Proc. Natl. Acad. Sci. USA* **107**, 12446 (2010).
- [15] C. R. Laumann, R. Moessner, A. Scardicchio, and S. Sondhi, Quantum annealing: The fastest route to quantum computation? *Eur. Phys. J.: Spec. Top.* **224**, 75 (2015).
- [16] V. N. Smelyanskiy, K. Kechedzhi, S. Boixo, S. V. Isakov, H. Neven, and B. Altshuler, Nonergodic delocalized states for efficient population transfer within a narrow band of the energy landscape, *Phys. Rev. X* **10**, 011017 (2020).
- [17] L. Faoro, M. V. Feigel’man, and L. Ioffe, Non-ergodic extended phase of the quantum random energy model, *Ann. Phys. (NY)* **409**, 167916 (2019).
- [18] M. Pino and J. J. Garcia-Ripoll, Mediator-assisted cooling in quantum annealing, *Phys. Rev. A* **101**, 032324 (2020).
- [19] M. Pino, J. Prior, and S. Clark, Capturing the re-entrant behavior of one-dimensional Bose–Hubbard model, *Phys. Status Solidi B* **250**, 51 (2013).
- [20] A. De Luca, B. L. Altshuler, V. E. Kravtsov, and A. Scardicchio, Anderson localization on the Bethe lattice: Nonergodicity of extended states, *Phys. Rev. Lett.* **113**, 046806 (2014).
- [21] E. Cuevas, V. Gasparian, and M. Ortuño, Anomalous large critical regions in power-law random matrix ensembles, *Phys. Rev. Lett.* **87**, 056601 (2001).
- [22] V. Kravtsov, B. Altshuler, and L. Ioffe, Non-ergodic delocalized phase in Anderson model on Bethe lattice and regular graph, *Ann. Phys. (NY)* **389**, 148 (2018).
- [23] G. Biroli and M. Tarzia, Anomalous dynamics on the ergodic side of the many-body localization transition and the glassy phase of directed polymers in random media, *Phys. Rev. B* **102**, 064211 (2020).
- [24] L. Colmenarez, D. J. Luitz, I. M. Khaymovich, and G. De Tomasi, Subdiffusive Thouless time scaling in the anderson model on random regular graphs, *Phys. Rev. B* **105**, 174207 (2022).
- [25] K. S. Tikhonov and A. D. Mirlin, Fractality of wave functions on a Cayley tree: Difference between tree and locally treelike graph without boundary, *Phys. Rev. B* **94**, 184203 (2016).
- [26] I. García-Mata, O. Giraud, B. Georgeot, J. Martin, R. Dubertrand, and G. Lemarié, Scaling theory of the Anderson transition in random graphs: Ergodicity and universality, *Phys. Rev. Lett.* **118**, 166801 (2017).
- [27] I. García-Mata, J. Martin, R. Dubertrand, O. Giraud, B. Georgeot, and G. Lemarié, Two critical localization lengths in the Anderson transition on random graphs, *Phys. Rev. Res.* **2**, 012020(R) (2020).
- [28] G. Biroli and M. Tarzia, Delocalization and ergodicity of the Anderson model on Bethe lattices, [arXiv:1810.07545](https://arxiv.org/abs/1810.07545).
- [29] G. Biroli, A. K. Hartmann, and M. Tarzia, Critical behavior of the Anderson model on the Bethe lattice via a large-deviation approach, *Phys. Rev. B* **105**, 094202 (2022).

- [30] A. D. Mirlin and Y. V. Fyodorov, Distribution of local densities of states, order parameter function, and critical behavior near the Anderson transition, *Phys. Rev. Lett.* **72**, 526 (1994).
- [31] A. D. Mirlin and Y. V. Fyodorov, Universality of level correlation function of sparse random matrices, *J. Phys. A* **24**, 2273 (1991).
- [32] K. Tikhonov and A. Mirlin, From Anderson localization on random regular graphs to many-body localization, *Ann. Phys. (NY)* **435**, 168525 (2021).
- [33] K. S. Tikhonov and A. D. Mirlin, Many-body localization transition with power-law interactions: Statistics of eigenstates, *Phys. Rev. B* **97**, 214205 (2018).
- [34] K. B. Efetov, Anderson metal-insulator transition in a system of metal granules: Existence of a minimum metallic conductivity and a maximum dielectric constant, *Zh. Eksp. Teor. Fiz* **88**, 1032 (1985) [*Sov. Phys. JETP* **61**, 606 (1985)].
- [35] M. R. Zirnbauer, Localization transition on the Bethe lattice, *Phys. Rev. B* **34**, 6394 (1986).
- [36] G. Biroli and M. Tarzia, Delocalized glassy dynamics and many-body localization, *Phys. Rev. B* **96**, 201114(R) (2017).
- [37] J. Edwards and D. Thouless, Numerical studies of localization in disordered systems, *J. Phys. C* **5**, 807 (1972).
- [38] A. Rodríguez, L. J. Vázquez, K. Slevin, and R. A. Römer, Critical parameters from a generalized multifractal analysis at the Anderson transition, *Phys. Rev. Lett.* **105**, 046403 (2010).
- [39] M. Ortuño, A. M. Somoza, and J. T. Chalker, Random walks and Anderson localization in a three-dimensional class C network model, *Phys. Rev. Lett.* **102**, 070603 (2009).
- [40] V. Hernandez, J. E. Roman, and V. Vidal, SLEPc: A scalable and flexible toolkit for the solution of eigenvalue problems, *ACM Trans. Math. Software* **31**, 351 (2005).
- [41] J. E. Roman and M. Pino, Large diagonalizations via polynomial filters in SLEPc: Application to eigenvectors of the Anderson model in a random-regular graph (unpublished).
- [42] M. Pino, Scaling up the Anderson transition in random-regular graphs, *Phys. Rev. Res.* **2**, 042031(R) (2020).
- [43] P. W. Anderson, Absence of diffusion in certain random lattices, *Phys. Rev.* **109**, 1492 (1958).
- [44] E. Abrahams, P. W. Anderson, D. C. Licciardello, and T. V. Ramakrishnan, Scaling theory of localization: Absence of quantum diffusion in two dimensions, *Phys. Rev. Lett.* **42**, 673 (1979).
- [45] A. Hagberg, P. Swart, and D. S. Chult, Exploring network structure, dynamics, and function using NetworkX, Los Alamos National Laboratory, Technical Report LA-UR-08-05495; LA-UR-08-5495, 2008 (unpublished).
- [46] P. Sierant, M. Lewenstein, and A. Scardicchio, Universality in Anderson localization on random graphs with varying connectivity, *SciPost Phys.* **15**, 045 (2023).
- [47] T. C. Halsey, M. H. Jensen, L. P. Kadanoff, I. Procaccia, and B. I. Shraiman, Fractal measures and their singularities: The characterization of strange sets, *Phys. Rev. A* **33**, 1141 (1986).
- [48] A. Rodríguez, L. J. Vázquez, K. Slevin, and R. A. Römer, Multifractal finite-size scaling and universality at the Anderson transition, *Phys. Rev. B* **84**, 134209 (2011).
- [49] L. Pausch, E. G. Carnio, A. Rodríguez, and A. Buchleitner, Chaos and ergodicity across the energy spectrum of interacting bosons, *Phys. Rev. Lett.* **126**, 150601 (2021).
- [50] J. Cardy, *Scaling and Renormalization in Statistical Physics*, Cambridge Lecture Notes in Physics Vol. 5 (Cambridge University Press, Cambridge, 1996).
- [51] M. Baroni, G. G. Lorenzana, T. Rizzo, and M. Tarzia, Corrections to the Bethe lattice solution of Anderson localization, [arXiv:2304.10365](https://arxiv.org/abs/2304.10365).
- [52] R. Abou-Chacra, D. Thouless, and P. Anderson, A self-consistent theory of localization, *J. Phys. C* **6**, 1734 (1973).
- [53] R. Andrae, T. Schulze-Hartung, and P. Melchior, Dos and don'ts of reduced chi-squared, [arXiv:1012.3754](https://arxiv.org/abs/1012.3754).